Scientia Iranica B (2015) 22(2), 539–560

Sharif University of Technology
Scientia Iranica
Transactions B: Mechanical Engineering
www.scientiairanica.com

Research Note

Mathematical modeling and optimization of the Electro-Discharge Machining (EDM) parameters on tungsten carbide composite: Combining response surface methodology and desirability function technique

S. Assarzadeh and M. Ghoreishi*

Department of Mechanical Engineering, K.N. Toosi University of Technology, Tehran, P.O. Box 19395-1999, Iran.

Received 18 June 2013; received in revised form 29 January 2014; accepted 6 September 2014

KEYWORDS
Electro-Discharge Machining (EDM);
Response Surface Methodology (RSM);
Multi-objective optimization;
Desirability Function (DF);
Tungsten carbide cobalt composite (WC-Co);
Process modeling.

Abstract. This research proposes a unified scheme to mathematically model and multi-objectively optimize the EDM parameters on tungsten carbide cobalt alloy (WC-6%Co), applying response surface methodology and a desirability function technique. Discharge current, pulse on-time, duty cycle and average discharge voltage have been chosen to be correlated with material removal rate, tool wear rate and surface roughness (Ra) as performance measures. The required experimental data were obtained in accordance with the face-centered central composite design. Significant parameters in the form of main, two-way interaction and pure quadratic effects were carefully identified conducting a complete analysis of variance at 1%, 5% and 7% significance levels, and the adequacy of all fitted second order regression models was confirmed. Parametric analysis was undertaken through direct and reciprocity effect plots to fully reveal the different facets of ED-machinability characteristics. Finally, the optimization issue has been formulated as multi-objective from which the optimal parametric setting, yielding the most enviable conditions simultaneously, was then obtained in a compromised manner employing the notion of a desirability concept. The predicted optimal results were also interpreted and verified experimentally. The values of relative validation errors are all quite satisfactory (below 11%), which prove the efficacy and reliability of the suggested approach.

1. Introduction

Electro-Discharge Machining (EDM) is an electro-thermal erosion process, where material is removed by a successive trend of controlled rapid and repetitive discrete electrical discharges (sparks), produced by a DC pulse generator, taking place between a pair of tool and work piece electrodes submerged in a liquid dielectric medium [1-3]. For decades, the process has achieved considerably popular applications in machining various engineering materials, especially High-Strength, Temperature-Resistant (HSTR) alloys (Inconel, Titanium, Beryllium alloys) [4-6], hard composites (metal matrix composites, nano-composites) [7,8], conductive ceramics [9], etc., and in miscellaneous industries, mostly, aeronautic, die, mould, and automobile industries, with its additional versatility being a very promising approach towards micro- as well as nano-machining technologies [10].

The literature reveals that a large amount of research work has mainly been focused on studying the EDM characteristics in different types of steel,

*. *Corresponding author. Tel.: +98 21 84063210; Fax: +98 21 88677274*
E-mail address: ghoreishi@kntu.ac.ir (M. Ghoreishi)

using either different combinations of tool materials or process modification, with some conventional routines, known as hybrid machining techniques, to enhance process productivity and accuracy [1,2,11]. In this context, researchers have mainly applied statistically designed or soft-computing-based techniques to model and optimize process parameters and responses. However, unlike steel often chosen as a general option for work piece material in EDM applications, it has been postulated that the behavior of ceramic composites, such as tungsten carbide-cobalt composite, can be rather different in response to various parameters under the EDM process [9]. Tungsten carbide-cobalt composite, amongst the most widely used difficult-to-cut materials, is one of the most important engineering materials with extreme applications commonly employed in manufacturing carbide dies and molds, cutting tools, forestry tools, and components resisting continual wear in production lines. Its acutely high hardness and strength, superior wear and corrosion resistance over a wide range of temperatures has frustrated conventional machining processes in being utilized efficiently in shaping such a material. Although the EDM process has now been recognized and justified as the best and perhaps the only proficient machining candidate for cutting and shaping tungsten carbides, the process is not an easy going task [3,12]. The main difficulty in EDMing WC-Co originates from its non-homogeneous structure, the differences between the melting and evaporation points of the two constituent phases present in its micro-structure, i.e. WC and Co grains, which may cause non-uniformity in erosion as well as process instability, producing short circuits and arcing pulses more frequently [12]. The melting and vaporization points of WC are about 2800°C and 6000°C, respectively, and those for Co are about 1320°C and 2700°C, both at normal atmospheric pressure [13,14]. Hence, during the EDM, the cobalt matrix first starts being removed from the surface by melting and evaporation mechanisms due to sparking. This early selective decomposition of the WC-Co structure will lead to dislodging coarse WC grains into the gap space, increasing the risk of process instability as a result of high debris accumulation and pollution inside the gap region. Moreover, there is a noticeable difference in the thermal expansion coefficient of WC and Co, the latter possessing a much higher one (14×10^{-6} 1/°C for Co as compared to 5×10^{-6} 1/°C for WC) [14]. The discrepancy is responsible for developing high thermal tension stresses during re-solidification and quenching, exceeding the fracture strength of the material in the crater, and thus, causing an abundance of cracks on the surface layer. For these reasons, the electro discharge machining of WC-Co composite is regarded as a challenging task imposing more difficulties compared to EDMing different kinds of hardened steels commonly studied in research articles.

1.1. *Literature review*

Lee and Li [15] studied the effects of EDM parameters on the surface characteristics of a kind of tungsten carbide. They concluded that the MRR and surface roughness of the work piece are directly proportional to the discharge current intensity. In further research [16], they undertook a comprehensive qualitative analysis of the surface integrity of ISO standard P-grade tungsten carbide under EDM conditions with peak current and pulse on-time variations. Miscellaneous aspects of surface integrity, like micro-cracks, recast layer formation and surface roughness, were studied. It was pointed out that the quality of the work surface is a function of two main parameters, peak current and pulse duration, both of which are settings of the power supply. In a more quantitative manner, Puertas et al. [17] applied a 2^3 full factorial design with four center points to provide protection against curvature in the model building of EDMing 94WC-6Co ceramic composite solely under finishing stages. Although different significant main and interaction effects between input parameters were identified using ANOVA, and their variations over selected responses were studied, neither definite input settings nor a numerical value of machining factors were obtained as optimum values, since no suitable optimization strategy was then tried. Once more, the same previous authors [18] conducted a comparative study of the die sinking EDM of three different conductive ceramics, viz. WC-Co, B_4C, and SiSiC in terms of MRR, Ra, and TWR as response technological variables, using the same aforementioned DOE plan under only a finishing regime, using low discharge energy levels. They indicated that the investigated ceramic materials showed different behaviors in response to the alterations of input factors, except for the MRR function, which manifested the same trend for all the work piece materials. In another study, Lin et al. [19] investigated the effects of electrical discharge energy on the machining characteristics of two kinds of cemented tungsten carbide, grades $K10$ and $P10$. They pointed out that there exists a particular range of machining parameters within which the process is stable, and exceedingly long or short pulse duration causes instability. As a soft computing based optimization strategy, Kanagarajan et al. [20] employed non-dominated sorting genetic algorithm (NSGA-II) to obtain a Pareto optimal series of input variables in a tradeoff manner. However, neither the role of pulse off-time as an independent variable nor the inclusion of tool wear phenomenon as an important response was taken into account, as both can definitely affect the process productivity, cost, and dimensional accuracy of machined parts. Once more, Kanagarajan et al. [21]

applied RSM, along with multiple linear regression analysis, to obtain second order response equations for MRR and Ra in EDMing WC/30%Co composite. Though the most influential parameters aiming at maximizing MRR and minimizing Ra were identified by carefully examining the surface and contour plots of the responses, again, their suggested approach suffers from the same aforementioned drawbacks. Banerjee et al. [22] applied a Face-Centered Central (FCC) composite design to collect experimental data and RSM to model and analyze the processing parameters involved in EDMing WC-TiC-TaC/NbC-Co cemented carbide. They found that sufficient superheating of work piece material and subsurface boiling are essential for efficient material removal, and that the formation of pock marks due to the bursting of blisters and associated crack formations may be controlled by choosing a proper combination of dielectric and interfering influential parameters. Finally and most recently, Puertas and Luis [23] studied the behavior of two highly practical conductive ceramics in industry, B_4C and WC-Co under different die sinking EDM conditions. Though practical recommendations on how to adjust process settings to acquire low surface roughness, low electrode wear, and high MRR were suggested independently, neither a precise optimization strategy nor a definite numerical parametric setting was then proposed to tradeoff between those conflicting objective responses, as they were treated autonomously from each other without considering their mutual interdependencies.

1.2. Structure and contributions of the current research

Based on the previously stated information in opening the basic subject and reviewing related past research, the major motivation of the present study is to fully understand and characterize the machinability measures of WC-6%Co in a more quantitatively systematic way in order to identify the correct effects of various interfering parameters influencing process responses. In this regard, the face-centered Central Composite Design (CCD) of experiments has been adopted to plan the experiments. Adequately sufficient second order response equations, i.e. MRR, TWR, and Ra, are developed based on RSM, using multiple linear regression analysis, along with ANOVA, in which both significant main and two-factor interactive effects are presently pre-documented by student t-tests. Subsequently, the mathematical forms of process responses are optimized to yield the best operating parameter combinations, satisfying the highest possible MRR, lowest TWR and Ra, simultaneously, in a compromised manner, using an aggregated desirability function idea. The foremost merits of the current research can be mentioned as follows:

a) By far, to the best of the authors' knowledge acquired through extensive review of related literature, the *simultaneous numerical optimization* of MRR, Ra, and TWR in the EDM of tungsten carbide has not yet been implemented. In the bibliography consulted, there is still a lack of practical knowledge on EDMing WC-Co, as few technological tables useful for both EDM practitioners and academicians can be found compared to those widely available for miscellaneous kinds of hardened steel.

b) Despite the fact that several experimental works have been directed towards studying EDMing WC-Co from different aspects [12], in their best cases, they have either ended at the point of merely developing respective responses without any attempt to highlight exact numerical optimal conditions [19], or obtaining optimal conditions without bearing in mind the possible interdependencies of all three main outputs (MRR, TWR, and Ra) at the same time, as one of which has often been neglected [20,21,23]. In addition, no effort has yet been put into applying the desirability function method, aiming to optimize the EDM parameters of WC-6%Co composite.

2. Experimental details

2.1. Machine tool, tool electrode, work piece and dielectric materials

An Azarakhsh ZNC spark erosion machine, model number 204, has been used to run the experiments. Equipped with an iso-frequency pulse generator, it can produce pulse-on times in the range 2μs-1000μs and provide maximum discharge current up to 75 A. Tungsten carbide cobalt composite, type WMG10, manufactured by the Wolframcarb Company, Italy, available in cylindrical form with 12 mm diameter, has been selected as the work piece material for all tests. The selected WC-Co composite, produced via powder metallurgy, having about 94%wt WC and 6%wt Co as its nominal chemical composition, is of a fine grain type and mainly used in fabricating drawing dies and woodworking tools, as well as cutting tools for nonferrous metals. Table 1 lists the relevant work piece material properties.

Electrolytic copper rods with the same diameter as the work piece were used for the tool electrode material. The physical and mechanical properties are a density of 8.9 g/cm^3, thermal conductivity 226 W/mK, electrical resistivity 9 $\mu\Omega$cm, melting point 1083°C, and hardness of about 100 HB. Copper has the additional advantage of being easily available, stable in quality and cheap compared to other applicable metals. The EDM experiments were all conducted in a planing mode in which both the tool and work piece bottom

Table 1. Work piece thermo-physical and mechanical properties.

Material composition	WC-6%wtCo (Iso grade: K10)
Hardness (HRA)	92.5
Melting point (°C)	2870
Boiling point (°C)	6000
Density (g/cm^3)	14.3
Transverse strength (MPa)	1700
Compressive strength (MPa)	6200
Modulus of Elasticity (GPa)	620
Thermal conductivity (Wm^{-1}K^{-1})	79.6
Thermal expansion coefficient (1/°C)	5.5×10^{-6}
Electrical resistivity (nΩm)	200

(a)

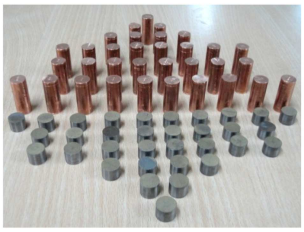

(b)

Figure 1. (a) Picture of Azarakhsh ZNC 204 EDM machine, and (b) work/tool electrode samples.

surfaces were ground, prior to experimentation, to remove any possible machining marks or irregularities, and assuring consistent initial gap width and flushing action. Moreover, commercial grade kerosene ejected as impulse side flushing through a nozzle was used as the dielectric liquid carrying out machining debris from the gap zone. Also, the tool and work piece electrode polarity were assigned as positive and negative, respectively, as this status can make tool wear minimum, along with having stable sparking [9]. Figure 1(a) and (b) show a photograph of the EDM machine and work piece/tool samples used in experiments.

2.2. Machining parameters, design of experiments, and measurements

Four controllable input variables, namely, discharge current (A: Amp), pulse-on time (B: μs), duty cycle (C: %), and average gap (reference) voltage (D: Volt) have been selected as predominant factors, based on the EDM machine operating characteristics and by consulting the respective bibliography [1,2], being the most effective parameters governing discharge energy, which directly affects process performance and efficiency.

The face-centered central composite design [24-26], a popular variant of the Central Composite Design (CCD) of experiments, has been employed to plan the experiments. It is a kind of second order design class, which uses three levels for each parameter and can efficiently handle linear, quadratic, as well as interaction terms, in process modeling. Generally, to collect enough data to establish a suitable second order regression response equation for a process involving k variables, the following three sets of design points are needed:

(a) $n_f = 2^k$ factorial design or corner points;

(b) $n_a = 2k$ axial or star points; and

(c) n_c center points, which are usually repeated several times to obtain a good estimation of experimental pure error.

The factorial points contribute in a major way to the estimation of linear and two-factor interaction terms, while axial points contribute in a large way to the estimation of quadratic terms. The center runs will also provide an internal estimate of error (pure error) and contribute to the prediction of quadratic terms [24-26].

To obtain a proper second order response surface equation, these are the minimum as well as optimum number of experimental runs. Though other approaches, such as the Taguchi design technique, which may need a smaller number of trails, can be applied, it suffers from serious drawbacks, the most important of which is its inability to obtain all the possible interaction effects [24-26]. Identifying and obtaining all interaction terms can be of vital importance in process modeling and optimization, and CCD assures such a trend [24-26].

Therefore, the total number of experiments would be:

$$N = n_f + n_a + n_c = 2^k + 2k + n_c. \qquad (1)$$

The location of axial points in a response surface central composite design, with respect to the center point (origin), is determined by alpha (α) value. The choice of α depends, to a great extent, on the domain of operation and interest [25]. In face-centered central composite design, $\alpha = 1$, meaning a three-level design space, coded as -1, 0, and 1, corresponds to low, medium, and high parameter levels, respectively. To specify the actual levels of each input variable, at first, a number of preliminary tests were conducted as a One-Factor-At-a-Time (OFAT) approach to determine the most stable combination of parameter settings over the operability region of the EDM machine [27]. Table 2 summarizes the relevant machining conditions and fixed parameters, whereas Table 3 lists the preferred

Table 2. The EDM conditions.

Working condition	Description
Workpiece material	WC-6%Co
Tool material	Commercial electrolytic copper
Polarity	Workpiece (-), tool (+)
Tool and workpiece dimensions	Cylindrical, Φ 12 mm
Peak current	2-8 A
Pulse-on time	50-150 μs
Duty cycle	40-80%
Gap voltage	40-80 V
Dielectric fluid	Commercial kerosene
Dielectric flow rate	5 L/min
Flushing pressure/type	1 MPa/side flushing
ED-machining time	60-90 min

Table 3. Independent input factors and levels for the face-centered CCD.

Parameter	Notation	Unit	Coded/Actual level		
			-1	0	+1
Discharge current (I)	A	Ampere	2	5	8
Pulse on-time (T_{on})	B	μs	50	100	150
Duty Cycle (DC)	C	-	40	60	80
Gap voltage (V)	D	Volt	40	60	80

input controllable parameters, along with their ranges in both coded and actual format.

The response variables were then chosen as material removal rate (MRR: g/h), tool wear rate (TWR: g/h), and average surface roughness (Ra: μm). Both the stock removal rate and tool wear rate were measured directly by the weight loss method, weighing the work piece and tool electrode samples before and after each test and dividing the corresponding weight difference by the elapsed time allocated for each experimental run. A GX-200 digital single pan balance, manufactured by the A&D Company, Japan, with a precision of 0.001 g and maximum capacity of 210 g, has been used for the evaluation. During the running of the first round of experiments, it was revealed that much longer times were needed to get a reasonable idea about the MRR [27]. So, the time allocated to each trial was at least an hour, and much longer times were considered for runs with lower discharge currents. Characterization of each work piece surface condition was conducted in terms of arithmetic mean deviations of the roughness profile from the central line along the measurement path. A Mahr-PS1 unit, a portable stylus type profilometer made-up by the Mahr Company, Germany, was used for roughness assessments. Before measuring surface roughness, each machined sample was cleaned in acetone liquid and dried with a cold air blower. To achieve validity and accuracy, each Ra measurement was repeated twice along two different directions, as there is no specific pattern for spark distribution over the work area. The average of the two replications was then assigned as the roughness value for each treatment combination. In all cases, a cutoff length of 0.8 mm and an evaluation length of 4 mm (5 × 0.8 mm) were adjusted on the unit, according to ISO 4287/1.

By repeating seven center points, the total number of conducted experiments for $k = 4$ was $2^4 + 2(4) + 7 = 31$, and are shown in Table 4, along with the corresponding process responses. The linear relationship between coded and actual values, in Tables 3 and 4, is as follows:

Discharge current:

$$A = [I - (I_{\max} + I_{\min})/2] / (I_{\max} - I_{\min})/2.$$

Pulse on-time:

$$B = [T_{\text{on}} - (T_{\text{onmax}} + T_{\text{onmin}})/2] / (T_{\text{onmax}} - T_{\text{onmin}})/2.$$

Duty cycle:

$$C = [\text{DC} - (\text{DC}_{\max} + \text{DC}_{\min})/2] / (\text{DC}_{\max} - \text{DC}_{\min})/2.$$

Gap voltage:

$$D = [V - (V_{\max} + V_{\min})/2] / (V_{\max} - V_{\min})/2,$$

Table 4. Design layout and experimental results.

Exp. no.	Run no.	Input process parameters								Response variables				
		Coded				Actual								
		A	B	C	D	I (A)	T_{on} (μs)	D.C. (%)	V (v)	MRR (g/h)	TWR (g/h)	Ra_1 (μm)	Ra_2 (μm)	Ave. Ra (μm)
1	4	-1	-1	-1	-1	2	50	40	40	0.067	0.013	4.203	4.182	4.193
2	24	1	-1	-1	-1	8	50	40	40	0.54	0.09	3.533	3.689	3.611
3	10	-1	1	-1	-1	2	150	40	40	0.04	0.007	5.280	5.169	5.225
4	30	1	1	-1	-1	8	150	40	40	0.26	0.05	5.395	5.988	5.692
5	7	-1	-1	1	-1	2	50	80	40	0.153	0.027	3.673	3.508	3.591
6	28	1	-1	1	-1	8	50	80	40	0.86	0.15	4.292	4.606	4.048
7	15	-1	1	1	-1	2	150	80	40	0.097	0.014	5.149	5.449	5.299
8	1	1	1	1	-1	8	150	80	40	0.62	0.1	5.670	5.935	5.803
9	20	-1	-1	-1	1	2	50	40	80	0.02	0.013	3.712	3.769	3.741
10	11	1	-1	-1	1	8	50	40	80	0.12	0.04	4.203	4.286	4.245
11	27	-1	1	-1	1	2	150	40	80	0.04	0.007	4.488	4.404	4.446
12	8	1	1	-1	1	8	150	40	80	0.2	0.04	6.159	6.563	6.361
13	23	-1	-1	1	1	2	50	80	80	0.147	0.027	3.642	3.649	3.646
14	12	1	-1	1	1	8	50	80	80	0.672	0.132	4.424	4.633	4.529
15	6	-1	1	1	1	2	150	80	80	0.067	0.007	4.777	4.790	4.784
16	26	1	1	1	1	8	150	80	80	0.44	0.09	6.907	6.271	6.589
17	18	-1	0	0	0	2	100	60	60	0.080	0.02	5.154	5.362	5.258
18	2	1	0	0	0	8	100	60	60	0.48	0.09	4.713	4.766	4.740
19	22	0	-1	0	0	5	50	60	60	0.368	0.064	3.329	3.461	3.395
20	14	0	1	0	0	5	150	60	60	0.216	0.032	5.902	6.014	5.958
21	5	0	0	-1	0	5	100	40	60	0.152	0.024	5.630	5.368	5.499
22	29	0	0	1	0	5	100	80	60	0.36	0.048	4.254	4.817	4.536
23	17	0	0	0	-1	5	100	60	40	0.344	0.056	4.632	4.726	4.679
24	25	0	0	0	1	5	100	60	80	0.232	0.04	5.056	5.278	5.167
25	9	0	0	0	0	5	100	60	60	0.272	0.04	5.645	5.448	5.547
26	21	0	0	0	0	5	100	60	60	0.280	0.048	4.658	4.519	4.589
27	13	0	0	0	0	5	100	60	60	0.296	0.048	4.675	4.632	4.654
28	31	0	0	0	0	5	100	60	60	0.288	0.04	5.177	5.283	5.230
29	16	0	0	0	0	5	100	60	60	0.272	0.04	4.840	4.557	4.699
30	19	0	0	0	0	5	100	60	60	0.264	0.048	4.821	5.153	4.987
31	3	0		0 0	0	5	100	60	60	0.272	0.048	5.632	5.495	5.564

where A, B, C and D are the coded values of variables I, T_{on}, DC, and V, respectively, I_{max}, T_{onmax}, DC_{max}, and V_{max} represent the maximum values of I, T_{on}, DC, and V, respectively, and, I_{min}, T_{onmin}, DC_{min}, and V_{min} are the corresponding minimum values of process parameters in each interval. Finally, it is to be noted that the order of experimentation was randomized, according to the second column of Table 4, to avoid the creeping effect of any possible extraneous or nuisance factors into the results [24].

3. Response surface modeling of process outputs

The practical optimization of EDM parameters on WC-Co composite necessitates the accurate model building of the process responses describing its behavior and characteristics under different operating conditions. Response Surface Methodology (RSM) [24-26], a collection of mathematical and statistical techniques aimed at developing suitable second order polynomial models, relating a number of input variables to selected responses by multiple linear regression analysis, has been employed here. The model, in terms of the observations, in matrix notation, is:

$$\mathbf{y} = \mathbf{X}\boldsymbol{\beta} + \varepsilon, \tag{2}$$

where $\mathbf{y}$ is a $(n \times 1)$ vector of observations (n is the number of observations), $\mathbf{X}$ is an $(n \times p)$ matrix of the levels of the independent variables ($p = k + 1$, k is the number of process variables or regressors), $\boldsymbol{\beta}$ is a $(p \times 1)$ vector of the regression coefficients and $\boldsymbol{\varepsilon}$ is an $(n \times 1)$ vector of random errors. The vector of fitted values, $\hat{y}_i$, corresponding to the observed values, y_i (fitted regression model), is then [25]:

$$\hat{\mathbf{y}} = \mathbf{X}\hat{\boldsymbol{\beta}}, \tag{3}$$

where $\hat{\boldsymbol{\beta}}$ is the least squares estimator of regression coefficients ($\boldsymbol{\beta}$) $[\beta_0, \beta_1, \beta_2, ..., \beta_k]^T$, and can be calculated based on the following equation:

$$\hat{\boldsymbol{\beta}} = (\mathbf{X}'\mathbf{X})^{-1}\mathbf{X}'y. \tag{4}$$

In the above equation, $\mathbf{X}'$ is the transpose of matrix $\mathbf{X}$, $\mathbf{X}'\mathbf{X}$ is a $(p \times p)$ symmetric matrix, and $\mathbf{X}'\mathbf{y}$ is a $(p \times 1)$ column vector. Therefore:

$$\hat{\mathbf{y}} = \mathbf{X}\hat{\boldsymbol{\beta}} = \mathbf{X}(\mathbf{X}'\mathbf{X})^{-1}\mathbf{X}'y = \mathbf{H}\mathbf{y}. \tag{5}$$

The $n \times n$ matrix $\mathbf{H} = \mathbf{X}(\mathbf{X}'\mathbf{X})^{-1}\mathbf{X}'$ is usually called the hat matrix, which plays a central role in regression analysis and in mapping the vector of observed values into a vector of fitted values. The difference between the actual observed value, y_i and the corresponding fitted value, $\hat{y_i}$, is the residual, $e_i = y_i - \hat{y_i}$, a $(n \times 1)$ vector. The n residuals may be conveniently written in matrix notation as:

$$\mathbf{e} = \mathbf{y} - \hat{\mathbf{y}} = \mathbf{y} - \mathbf{X}\hat{\boldsymbol{\beta}} = \mathbf{y} - \mathbf{H}\mathbf{y} = (\mathbf{I} - \mathbf{H})\mathbf{y}, \tag{6}$$

where $\mathbf{I}$ is an $(n \times n)$ identity matrix. In scalar notation, the general form of a fitted response surface quadratic model can be written as:

$$\hat{y} = \beta_0 + \sum_{i=1}^{k} \beta_i x_i + \sum_{i=1}^{k} \beta_{ii} x_i^2 + \sum_{i=1}^{k-1} \sum_{j=i+1}^{k} \beta_{ij} x_i x_j. \tag{7}$$

The intercept coefficient, β_0, represents the response at the center of the experiments, where all the variables are zero (in coded form); β_i, β_{ii}, and β_{ij} also show the linear, quadratic, and linear-by-linear interaction effects of the parameters, respectively. This second-order polynomial is the most commonly used form and works quite well for a relatively small region of the variable space. By applying the Least Squares Method (LSM) [24-26], all these coefficients in a multiple regression model can be estimated.

In this study, the quantitative form of the relationship between desired responses and independent input variables can be represented by the following form:

$$y = f(I, T_{\mathrm{on}}, \mathrm{DC}, V), \tag{8}$$

where y is the desired response and f is the response function or surface. The steps consisting of applying regression analysis, performing pooled ANOVA on each obtained regression coefficients to find statistically significant terms, and finally, conducting ANOVA and some routine statistics to check modeling adequacy and goodness of fit, are the necessary actions needed to be carefully executed to find the suitable reduced quadratic forms of response functions, MRR, TWR, and Ra for the highly stochastic process of EDM. The next sections focus on these procedures.

3.1. Mathematical modeling of MRR, TWR, and Ra

Based on the model described by Eq. (8) and by applying the LSM, all the regression coefficients pertaining to the three responses have been obtained and are shown in Table 5, along with their corresponding Student T- and P-values as a pooled ANOVA format. As is clear from this table, all the main effects of four input parameters (A: discharge current, B: pulse on-time, C: duty cycle, and D: gap voltage) are found to be highly significant, at least at a $\alpha = 0.01$ significance level or 99% confidence interval, having almost zero P-values, in affecting both the MRR and TWR. However, for the third response, Ra, just the first two factors, discharge current (A) and pulse-on time (B) are regarded as the highly significant main factors. In the terminology of statistical modeling, the lower the P-value, the more influential is the effect [24-26]. On the other hand, the pure quadratic effect of duty cycle (C^2), the two-way interactions of discharge current with pulse-on time ($A \times B$), with duty cycle ($A \times C$), and with gap voltage ($A \times D$), as well as the interaction amongst the pulse on-time with duty cycle ($B \times C$), were also found to be extremely important terms influencing MRR. For the TWR measure, the dual interactive effects amid current with pulse-on time ($A \times B$), with duty cycle ($A \times C$), and with gap voltage ($A \times D$), plus pulse on-time and duty cycle ($B \times C$), along with the second order effects of discharge current (A^2) and duty cycle (C^2), were made known to have influencing outcomes. Finally, for the Ra quality measure, the only considerable interactive terms are the discharge current with pulse-on time ($A \times B$) and with gap voltage ($A \times D$). As a whole, the inclusion of any term with a P-value less than 0.07 designated as an upper bound for statistical significance, i.e. being significant within 93% of confidence interval, has been guaranteed in this research, so as to increase each model's accuracy

Table 5. Regression coefficients and T-test results for the individual MRR, TWR and Ra model parameters.

Predictor	MRR model			TWR model			Ra model		
	Coefficient	T-value	P-value	Coefficient	T-value	P-value	Coefficient	T-value	P-value
Constant	0.2790	80.939	0.0001[a]	0.0449	22.803	0.0001[a]	5.0082	38.649	0.0001[a]
A	0.2003	34.796	0.0001[a]	0.0359	22.957	0.0001[a]	0.3019	2.933	0.010[a]
B	-0.0631	-17.705	0.0001[a]	-0.0116	-7.416	0.0001[a]	0.8421	8.179	0.0001[a]
C	0.1029	17.869	0.0001[a]	0.01728	11.035	0.0001[a]	-0.0104	-0.101	0.920
D	-0.0527	-14.787	0.0001[a]	-0.0062	-3.939	0.001 [a]	0.0759	0.738	0.471
A^2	-0.0004	-0.058	0.954	0.0096	2.337	0.033[b]	0.0263	0.097	0.924
B^2	0.0116	1.602	0.137	0.0026	0.640	0.531	-0.2962	-1.092	0.291
C^2	-0.0244	-3.379	0.006[a]	-0.0094	-2.270	0.037[b]	0.0448	0.165	0.871
D^2	0.0076	1.048	0.317	0.0026	0.640	0.531	-0.0497	-0.183	0.857
AB	-0.0375	-7.249	0.0001[a]	-0.0054	-3.274	0.005[a]	0.2143	1.962	0.067[c]
AC	0.0718	10.074	0.0001[a]	0.0136	8.167	0.0001[a]	0.0841	0.770	0.453
AD	-0.0481	-9.306	0.0001[a]	-0.0051	-3.048	0.008[a]	0.2663	2.439	0.027[b]
BC	-0.0207	-4.002	0.002[a]	-0.0046	-2.747	0.014[b]	0.0454	0.416	0.683
BD	0.0067	1.687	0.120	0.0026	1.543	0.142	-0.0348	-0.319	0.754
CD	0.0080	1.539	0.152	0.0016	0.941	0.361	0.0459	0.421	0.680

[a]: Significant at $\alpha = 1\%$ significance level; [b]: Significant at $\alpha = 5\%$ significance level; [c]: Significant at $\alpha = 7\%$ significance level.

and adequacy as highly as possible. All the other terms not meeting such a criterion are supposed to be insignificant. Generally, the term "interaction" means that the effect of a factor over a known response depends on the level of another factor. Identifying significant interaction terms in the RSM model building procedure and their inclusions in the structure of a second order model are of vital importance, as they can reveal very crucial phenomena of the combinatorial joint effects of different process parameters on every process characteristic and behavior [24-26].

Removing insignificant terms is a common practice amongst empirical model builders which, in most cases, can result in improved model fitting capabilities, aside from yielding a simpler model form. Thus, the insignificant terms have been excluded from the model structures through a backward elimination method [24-26], and the ANOVA has been repeated for every obtained reduced quadratic model containing only those significant terms contributing to model building. Table 6 illustrates the ANOVA results for the three response functions. As desired, all the quadratic regression models are significant, while their lacks of fits turned out to be insignificant relative to pure error. Hence, the model adequacy checking is completely assured for each output measure. Other statistical diagnostic indices mainly used to evaluate the modeling goodness of fit are the ordinary R-squared (R^2), adjusted R-squared (R^2_{Adj}), and predicted R-squared (R^2_{Pred}) [26], shown in Table 6, for every response model. The values are 99.74%, 99.59%, and 98.51% for MRR; 97.58%, 96.38%, and 91.13% for TWR; and 80.93%, 77.12%, and 74.1% for Ra, respectively. As a general rule, the more the R^2s approach unity, the better the model fits the experimental data [24-26]. The usual statistic, R^2, also called the coefficient of multiple determination, indicates how many percent of the total variations can be explained by the model, while the R^2_{Adj}, a statistic adjusted for the size (the number of factors) of the model, means how many percent of the total variability can be explained by the model after considering the significant terms (reduced model). The amount of R^2 increases as each additional variable or regressor, whether significant or insignificant, is added to the model. On the contrary, the adjusted R^2 does not automatically increase when new predictor variables are added to the model. In fact, the value of adjusted R^2 will often decrease when unnecessary terms are included. Accordingly, when R^2 and R^2_{Adj} differ dramatically, there is a good chance that non-significant terms have been incorporated in the model [24-26]. Therefore, it is a suitable criterion in evaluating a model's goodness of fit when only significant terms are involved, compared to the case when all the terms are caught up. The statistic PRESS (prediction error sum of squares) is a measure of how well the model will predict new data. A model with a small value of PRESS is desired, as it indicates that the model is likely to be a good predictor [25]. In connection with this, the predicted R^2 (R^2_{Pred}) is defined, which is an indication of the predictive capability of the regression model in response to new observations.

The R^2s coefficients and PRESS statistic are

Table 6. ANOVA table for the trimmed MRR, TWR and Ra second order models.

Source	DF	Seq SS	Adj MS	F value	P value	Remarks
(a) For MRR						
Regression	9	1.05761	0.11751	676.09	0.000	Significant
Linear	4	0.98063	0.22721	1307.20	0.000	
Square	1	0.00825	0.00066	3.79	0.069	
Interaction	4	0.06874	0.01718	98.86	0.000	
Residual error	16	0.00278	0.00017	-	-	
Lack-of-fit	10	0.00250	0.00021	1.68	0.271	Insignificant
Pure error	6	0.00073	0.00012	-	-	
Correlation total	25	1.06039	-	-	-	
$R^2 = 99.74\%$ $R^2_{\text{Adj}} = 99.59\%$ $R^2_{\text{Pred}} = 98.51\%$ PRESS $= 0.01577$						
(b) For TWR						
Regression	10	0.03641	0.00364 8	0.76	0.000	Significant
Linear	4	0.03174	0.00794	176.02	0.000	
Square	2	0.00051	0.00025	5.64	0.011	
Interaction	4	0.00415	0.00104	23.07	0.000	
Residual error	20	0.00090	0.00005	-	-	
Lack-of-fit	14	0.00079	0.00006	3.09	0.086	Insignificant
Pure error	6	0.00011	0.00002	-	-	
Correlation total	30	0.03731	-	-	-	-
$R^2 = 97.58\%$ $R^2_{\text{Adj}} = 96.38\%$ $R^2_{\text{Pred}} = 91.13\%$ PRESS $= 0.00331$						
(c) For Ra						
Regression	5	16.379	3.2758	21.22	0.000	Significant
Linear	3	14.510	4.8365	31.33	0.000	
Interaction	2	1.870	0.9348	6.06	0.007	
Residual error	25	3.859	0.1544	-	-	
Lack-of-fit	9	1.942	0.2158	1.80	0.146	Insignificant
Pure error	16	1.917	0.1198	-	-	
Correlation total	30	20.239	-	-	-	
$R^2 = 80.93\%$ $R^2_{\text{Adj}} = 77.12\%$ $R^2_{\text{Pred}} = 74.10\%$ PRESS $= 5.24248$						

calculated as [25]:

$$R^2 = \frac{\text{SS}_R}{\text{SS}_T} = 1 - \frac{\text{SS}_{\text{Res}}}{\text{SS}_T}, \tag{9}$$

$$R^2_{\text{Adj}} = 1 - \frac{\text{SS}_{\text{Res}}/(n-p)}{\text{SS}_T/(n-1)} = 1 - \frac{\text{MS}_{\text{Res}}}{\text{MS}_T} = 1 - \left(\frac{n-1}{n-p}\right)(1-R^2), \tag{10}$$

$$R^2_{\text{Pred}} = 1 - \frac{\text{PRESS}}{\text{SS}_T}, \tag{11}$$

$$\text{PRESS} = \sum_{i=1}^{n} e^2_{(i)} = \sum_{i=1}^{n} \left[y_i - \hat{y}_{(i)}\right]^2, \tag{12}$$

where SS_R is the regression sum of squares, SS_T is the total sum of squares, SS_{Res} is the residual sum of squares, MS_{Res} is the residual mean square, MS_T is the total mean square, and $\hat{y}_{(i)}$ is the predicted value of the ith observed response based on a model fit to the remaining $(n-1)$ sample points.

A broad overview of these indices confirms the suitability and completeness of all the obtained models, as neither inconsistency nor poor adequacy can be observed. A complete residual analysis has also been undertaken for every developed response and the graphs are shown in Figure 2(a)-(c). A normal probability plot of residuals reveals that experimental data are spread approximately along a straight line, confirming a good correlation between experimental and predicted values for the response (Figure 2, a(A), b(A), and c(A)). In the graph of residuals versus fitted values (Figure 2, a(B), b(B), and c(B)), only small variations can be seen. The histogram of residuals (Figure 2, a(C), b(C), and c(C)) also shows a Gaussian

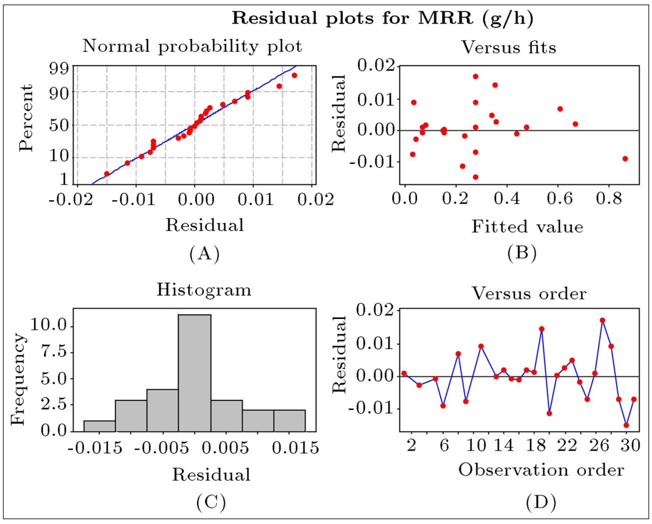

(a)

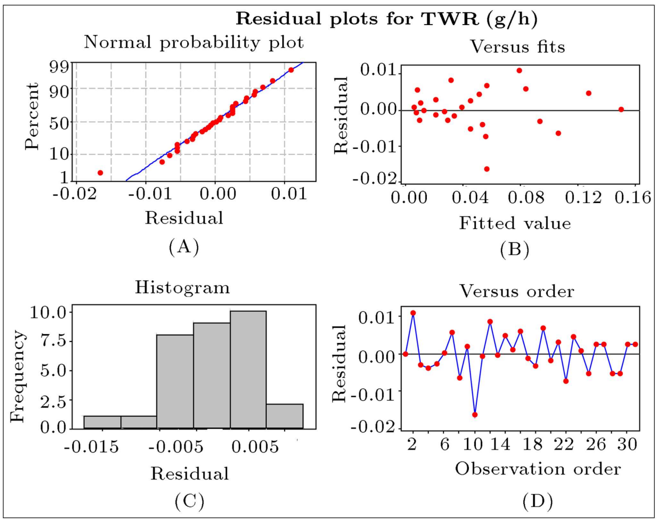

(b)

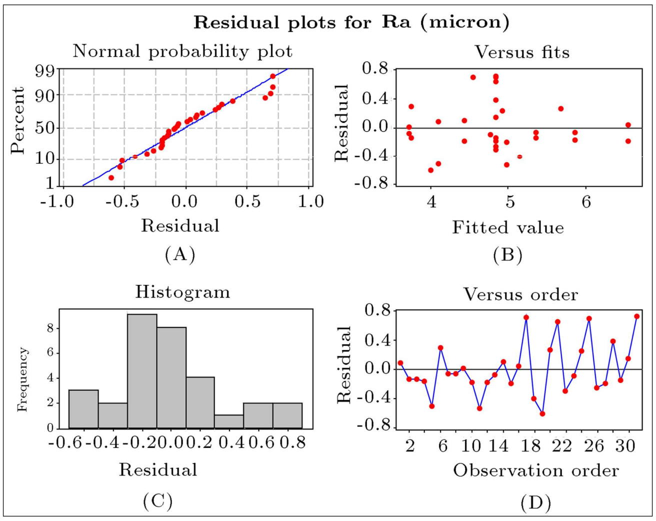

(c)

Figure 2. Plot of residuals: (a) MRR; (b) TWR; and (c) Ra. (A) normal probability plot of residuals; (B) residuals versus the fitted values; (C) histogram of the residuals; and (D) residuals against the order of data.

distribution, which is desirable. Finally, in residuals against the order of experimentations in Figure 2, a(D), b(D), and c(D), both negative and positive residuals are apparent, indicating no special trend, which is worthy from a statistical point of view. As a whole, all the yielded models show no inadequacy.

Table 7 details all the numerical values of finalized individual regression coefficients for every response. Based on these, the mathematical equations are conformed for each performance characteristics to be suitable coefficients and can be expressed in terms of coded factors as:

$$\begin{aligned}\mathrm{MRR} =&0.282 + 0.194A - 0.063B + 0.11C - 0.051D\\ &- 0.014C^2 - 0.041A \times B + 0.076A \times C\\ &- 0.042A \times D - 0.017B \times C,\end{aligned} \tag{13}$$

$$\begin{aligned}\mathrm{TWR} =&0.045 + 0.036A - 0.012B + 0.017C\\ &- 0.006D + 0.012A^2 - 0.007C^2\\ &- 0.005A \times B + 0.014A \times C - 0.005A \times D\\ &- 0.005B \times C,\end{aligned} \tag{14}$$

$$\begin{aligned}\mathrm{Ra} =&4.849 + 0.302A + 0.842B + 0.076D\\ &+ 0.214A \times B + 0.266A \times D.\end{aligned} \tag{15}$$

The above developed models can be used as reliable tools navigating the design space within the process parameters domain to get an in-depth understanding of process characteristics, and can also be utilized in the optimization stage to find optimum EDMing conditions on WC-6%Co.

Table 7. Finalized regression coefficients of the response models.

Coefficient	MRR (g/h)	TWR (g/h)	Ra (μm)
β_0 (intercept)	0.2819	0.0454	4.8486
β_A	0.1937	0.0359	0.3019
β_B	-0.0631	-0.0116	0.8421
β_C	0.1096	0.0173	Insignificant
β_D	-0.0510	-0.0062	0.0759*
β_{A^2}	Insignificant	0.0119	Insignificant
β_{C^2}	-0.0139	-0.0071	Insignificant
β_{AB}	-0.0413	-0.0054	0.2143
β_{AC}	0.0755	0.0136	Insignificant
β_{AD}	-0.0423	-0.0051	0.2663
β_{BC}	-0.0168	-0.0046	Insignificant

* The effect of gap voltage (D) on surface roughness is insignificant (see Table 5) and its coefficient has just been kept to comply with the *hierarchy* principle.

The EDM is an inherently stochastic and complex process, and it would be of interest to check the variability of output responses, i.e., MRR, TWR, and Ra, when an experiment is repeated using the same set of input parameter settings. It is also of great importance to test the generalization capabilities of developed models in response to some input data settings not used in the DOE plan but lying within the limits of input parameter domains. These investigations can helpfully provide fair justice to how robust the response surface models are in points of the reliability of gathered data used for model building, as well as models' predictive capabilities. Table 8 lists a set of five repetitive experimental runs selected randomly from Table 4, which account for checking the variability of output responses, while Table 9 presents a set of five additional tests, carefully designed to be different from those used for model building, to check the predictive accuracy of the developed models.

It is to be noted that the number shown in parenthesis in the first column of Table 8 corresponds to the experimental number in Table 4, for which the experimental setting has been repeated.

It can be inferred from Table 8 that there exists an acceptable level of variability when some experiments are repeated. The amounts of each two repetitive output responses are in close proximity to each other, assuring that the data base obtained from the adopted FCC design could reliably represent the EDM behavior of WC/6%Co under different conditions and could confidently be used for model development The average percentage deviations are 1.84%, 0.42%, and 15.3% for MRR, TWR, and Ra over these five repetitions, respectively. The values are obviously acceptable in view of engineering applications.

Table 9 illustrates the results of several confirmation experiments conducted to check the accuracy of each response model. The values of mean relative prediction errors are 8.75%, 10.30%, and 4.96% for MRR, TWR, and Ra, respectively. Therefore, it can be concluded that the obtained second-order response equations are quite adequate, possessing reasonable accuracy, to capture the highly nonlinear trends of EDM measures, and can satisfactorily be used for further analysis and optimization purposes.

4. Results and discussion

To genuinely describe the quality of variation trends of each process response with respect to inputs, it is of great importance to be aware that spark energy is the dominant factor most responsible for the mechanism of material removal in EDM. The amount of discharge energy (q) delivered per single discharge, assuming a normal pulse (i.e. spark), can be expressed as [28]:

$$q=\int_{T_d}^{T_{\mathrm{on}}} V_{\mathrm{dis}} I_{\mathrm{dis}} dt \approx V_{\mathrm{dis}}.I_{\mathrm{dis}}.(T_{\mathrm{on}}-T_d) \approx V_{\mathrm{dis}}.I_{\mathrm{dis}}.T_{\mathrm{on}}, \quad (16)$$

Table 8. Experimental checking of the repeatability of output response data.

Exp. no	Input process parameters				Response variables						Percentage variation* (%)		
	I (A)	T_{on} (μs)	DC (%)	V (v)	MRR_1 (g/h)	MRR_2 (g/h)	TWR_1 (g/h)	TWR_2 (g/h)	Ra_1 (μm)	Ra_2 (μm)	MRR	TWR	Ra
1 (4)	8	150	40	40	0.260	0.230	0.050	0.057	5.692	5.511	3	0.7	18.1
2 (9)	2	50	40	80	0.020	0.023	0.013	0.011	3.741	3.904	0.3	0.2	16.3
3 (17)	2	100	60	60	0.080	0.073	0.020	0.023	5.258	5.424	0.7	0.3	16.6
4 (20)	5	150	60	60	0.216	0.244	0.032	0.036	5.958	5.837	2.8	0.4	12.1
5 (24)	5	100	60	80	0.232	0.256	0.040	0.035	5.167	5.301	2.4	0.5	13.4
Mean percentage variation (%)											1.84	0.42	15.3

* Percentage variation (%) = $|R_1 - R_2| \times 100$, where R_1 and R_2 stand for the first and second repetition of each response, respectively.

Table 9. Experimental verification of response surface models.

Exp. no	Input process parameters				MRR (g/h)		TWR (g/h)		Ra (μm)		Relative* prediction error (%)		
	I (A)	T_{on} (μs)	DC (%)	V (v)	Experimental	Model	Experimental	Model	Experimental	Model	MRR	TWR	Ra
1	4	100	70	50	0.311	0.274	0.043	0.041	4.786	4.41 5	11.90	4.65	7.75
2	5	75	60	60	0.698	0.782	0.045	0.051	4.551	4.428	12.03	13.33	2.70
3	3	125	60	60	0.238	0.259	0.025	0.022	5.443	4.9 97	8.82	12	8.19
4	6	150	50	70	0.183	0.175	0.035	0.031	5.803	5.94 5	4.37	11.43	2.45
5	7	50	80	70	0.587	0.626	0.099	0.109	4.353	4.192	6.64	10.10	3.70
Mean relative prediction error (%)											8.75	10.30	4.96

* Relative prediction error (%) $= \left|\frac{\text{Experimental result}-\text{Predicted result}}{\text{Experimental result}}\right| \times 100$.

where T_d, T_{on}, V_{dis}, and I_{dis} represent the ignition delay time, pulse on-time, discharge voltage and current, respectively. The magnitude of ignition delay time in normal pulses is so small compared to pulse on-time [29], so its effects have been neglected for the sake of simplicity. Under real EDM conditions, for a sequence of electrical discharges occurring between the two electrodes within the total machining time (T), the total discharge duration (T_D) is given by:

$$T_D = T \times \text{DC}, \tag{17}$$

where DC is the duty cycle. On the other hand, the whole number of discharge pulses (N) during total machining time can be calculated as:

$$N = \frac{T}{T_{\text{on}} + T_{\text{off}}} = T \times \frac{T_{\text{on}}}{T_{\text{on}} + T_{\text{off}}} \times \frac{1}{T_{\text{on}}} = \frac{T \times \text{DC}}{T_{\text{on}}} = \frac{T_D}{T_{\text{on}}}. \tag{18}$$

Therefore, the total discharge energy (Q) during overall machining time is given by:

$$Q = q \times N = V_{\text{dis}}.I_{\text{dis}}.T_{\text{on}} \times \frac{T_D}{T_{\text{on}}} = V_{\text{dis}}.I_{\text{dis}}.T_D = V_{\text{dis}}\,.I_{\text{dis}}.T.\text{DC}. \tag{19}$$

This is the total electrical discharge energy delivered into the gap zone, which is then shared between the tool and work piece electrodes, as well as the dielectric liquid. All the following discussions are based on this simple relation describing the whole generated electro-thermal energy during sparking, expressed in terms of the selected input EDM parameters. In what follows, a comprehensive parametric analysis of the influence of input variables on output features is undertaken as main (direct) and interaction effect plots. In the first, one factor is varied from the minimum to maximum level, while other parameters are kept constant at their middle level. For the latter, the effect of a factor on the respective response is studied at different levels of another factor, while keeping all other variables unchanged.

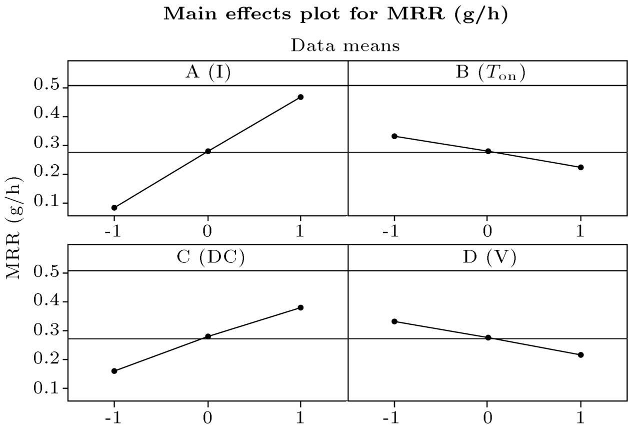

Figure 3. The main effects plot of input parameters over the MRR.

4.1. Main effect analysis of MRR

In this section, the direct effects of four selected input factors, namely, A: discharge current, B: pulse on-time, C: duty cycle, and D: gap voltage on Material Removal Rate (MRR) are studied independently. The plots obtained in this manner are called main effects plots, which are discussed in the following.

Figure 3 shows the main effect plot of each variable on the MRR. As is clear, the MRR increases steadily with the increase of discharge current. Higher levels of discharge currents result in stronger electrical discharges capable of removing a chunk of material from the work piece, hence, boosting the rate of erosion [30]. The MRR tends to decrease with the increase of pulse on-time. Despite the usual belief that longer pulse on-times provide much more time for electrical discharging compared to shorter ones, in reality, longer pulse durations cause the plasma channel to expand excessively, thus, lowering the plasma flushing efficiency and electrical discharge density within the gap space, with more molten material resolidifying instead of being effectively removed [31,32]. On the contrary, the main effect of the duty cycle displays a reverse tendency. At a constant level of pulse on-time ($B = 0$), increasing duty cycle means lowering the pulse off-time, thereby, decreasing the idle time between successive sparks, which produces higher discharging frequency, leading to a higher removal rate. Finally, it can be inferred from the main effect plot of gap voltage that higher MRR is attainable at lower levels of gap voltage. Higher gap voltage provides wider gap distance, which, in turn, results in diminished electrical discharge density and larger gap electrical resistivity, hindering the proper transmissivity of sparks [32]. So, the MRR decreases with the increase of gap voltage alone. It should be noted that these results have been acquired, considering the effect of each factor independently (keeping the other parameters unchanged). Nevertheless, more practically beneficial outcomes are revealed when their mutual joint effects are investigated simultaneously. This can be obtained by studying interaction effect plots drawn for each significant two-way interactive parameter over the relevant response.

4.2. Interaction effect analysis of MRR

Figure 4(a) depicts the combined effects of pulse on-time at different levels of discharge current over the MRR. It can be inferred that the maximum MRR is attainable at the lowest level of pulse on-time, along with the highest level of discharge current. This phenomenon can be best attributed to the increased energy density of discharge channel (J) relative to I and T_{on}, given by [33]:

$$J = k\frac{I^a}{T_{\text{on}}^b}, \tag{20}$$

where a, b and k are constant coefficients. Although the discharge energy itself is small with a short pulse on-time (Eq. 16), a higher discharge density is expected due to a very small discharge channel diameter. Hence, the higher the discharge current and the lower the pulse on-time, the larger is the electrical discharge density. Higher discharge density causes most of the material in the discharge area to be removed in the form of evaporation, with a thinner recast layer left on the work surface, increasing the plasma flushing efficiency [34], hence, MRR. Figure 4(b) illustrates the interactive effect duty cycle and current on MRR. It is understood that while keeping pulse on-time and gap voltage constant, higher amounts of MRR are achievable at the point of both larger discharge current and duty cycle. At a steady pulse on-time, an increased duty cycle implies lower pulse off-time and, when combined with elevated discharge current, a higher rate of electrical discharge energy is assured, making the MRR as large as possible. Figure 4(c) shows the

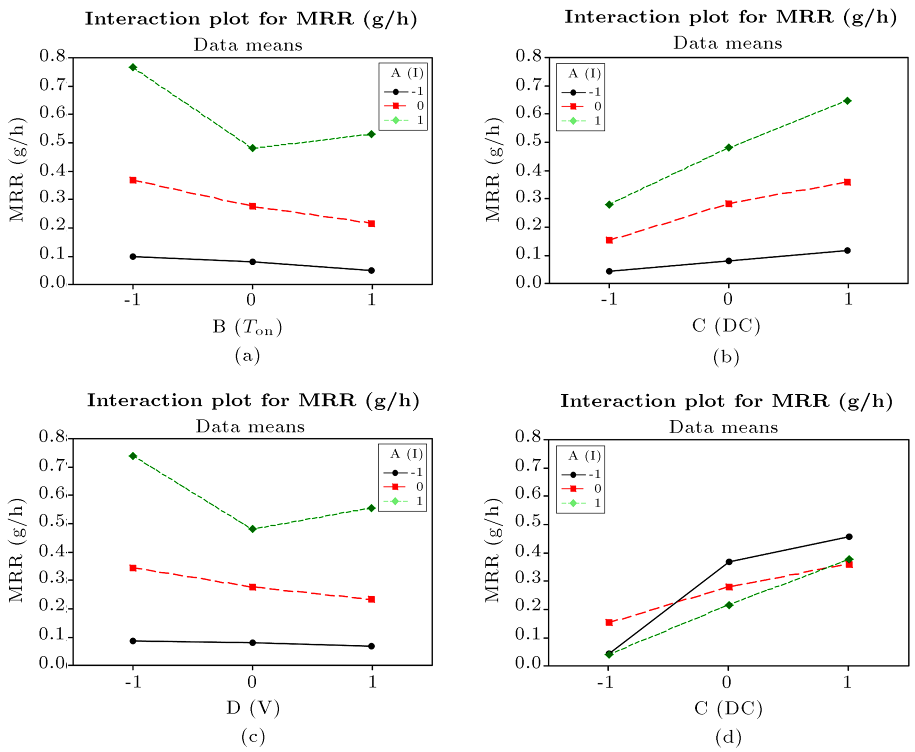

Figure 4. Interaction effect plots of MRR: (a) Pulse on-time (B) and discharge current (A); (b): duty cycle (C) and discharge current (A); (c) gap voltage (D) and discharge current (A); and (d) duty cycle (C) and pulse on-time (B).

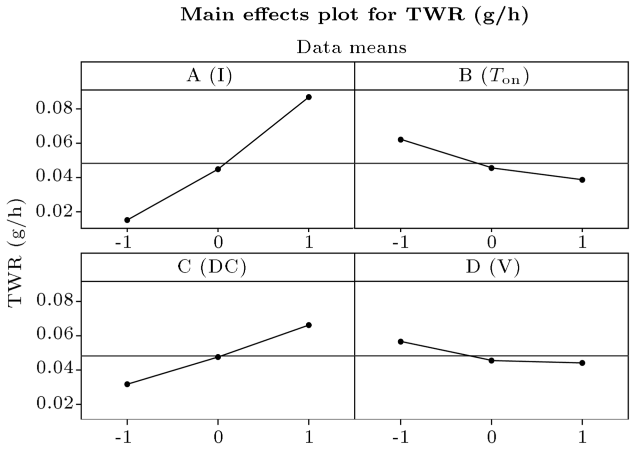

Figure 5. The main effects plot of input parameters over the TWR.

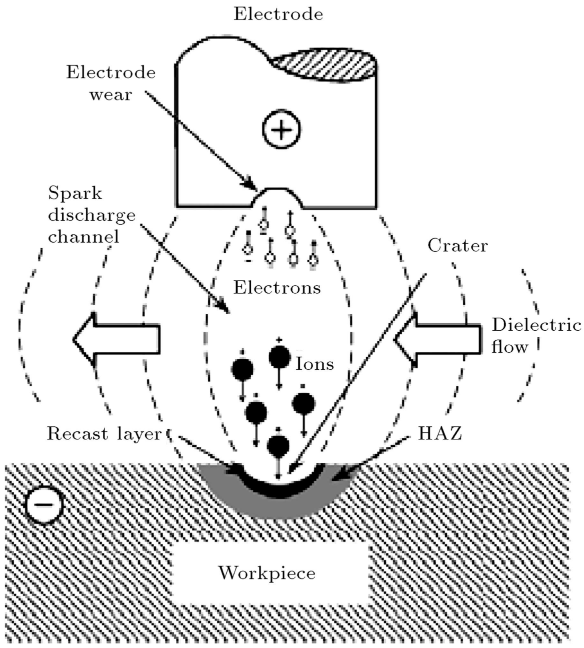

Figure 6. Schematic drawing of a single electrical discharge.

effect of gap voltage and current, whereas Figure 4(d) portrays the combined effect of duty cycle and pulse on-time over the MRR. It becomes clear that higher values of current, along with lower gap voltage, will definitely provide a suitable medium for higher rates of material melting and evaporation during sparking, thanks to enhanced electrical discharge density in a narrower gap region [31]. The lowest pulse on-time and highest duty cycle convey the greatest discharge frequency within the process input domain in which more material can be removed from the work piece in a unit time [35]. This event is clearly visible in Figure 4(d).

4.3. Main effect analysis of TWR

Figure 5 shows the main effect of each of four input parameters drawn, keeping the other factors constant at their middle level. A similar trend is observed compared to the main effects of MRR. The TWR tends to increase by increasing the discharge current and can reach up to about 0.09 g/h alone. This is the highest amount of TWR in these plots, which, in turn, confirms that the discharge current is paramount amongst other parameters in affecting the TWR. It is clear from the main effect plot of pulse on-time that setting longer pulse on-times can favor the TWR, as shorter pulse durations will deteriorate the tool wear. To better justify this fact, Figure 6 illustrates a schematic view of a single electrical discharge occurring between the two electrodes and the formed plasma channel. While keeping constant polarity, during every discharge, accelerated electrons bombard the surface of the anode (positive pole: tool), whereas ions aiming to move toward the cathode (negative pole: work piece) collide with the work surface. With small values of pulse duration, a higher number of negatively charged particles, being thousands of times lighter than ions, get the chance of being energized; stroking the positive (anode) tool electrode, and, thereby, increasing the rate of electrode material erosion [36,37]. On the same basis, the rising tendency of TWR with regard to duty cycle can be rationalized. A higher level of duty cycle is equivalent to lower pulse off-time and, hence, higher pulse frequency, which implies greater TWR due to the privileged rate of electron collisions with the anode tool surface [30]. On the other hand, selecting lower gap voltage results in larger amounts of tool wear. The same reason as mentioned for the MRR can surely be applied here, since a larger gap distance, while keeping other variables unchanged, will give rise to reduced electrical discharge density, which can less affect the tool electrode against wear.

4.4. Interaction effect analysis of TWR

The interaction effect plot of TWR, with regard to current and pulse on-time, has been depicted in Figure 7(a). As always smaller TWRs are demanded, they can be reached at lower discharge currents, followed by longer pulse on-times. A small discharge current provides lower discharge intensity (Eq. (16)), while prolonged pulse duration will give more chance for much heavier positive ions to reach the target cathode work piece, thus, occupying most of the plasma channel path and letting less excited electrons attack the anode tool [36].

Figure 7(b) shows the mutual effect of duty cycle and discharge current on TWR. It is noticeably revealed that smaller TWRs can, especially, be obtained by a combination of both low discharge current and duty cycle, and that much smaller TWRs are accomplished moving towards the minimum current. This fact, however, cannot be elicited solely by checking the main effect plots of the duty cycle and current, as both

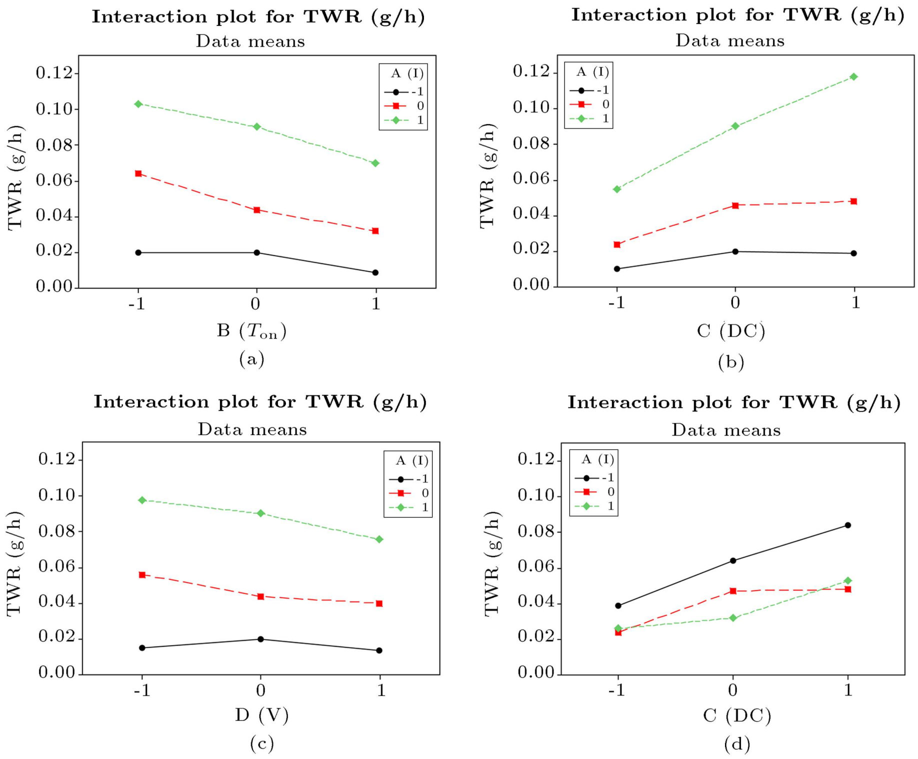

Figure 7. Interaction effect plots of TWR: (a) Pulse on-time (B) and discharge current (A); (b) duty cycle (C) and discharge current (A); (c) gap voltage (D) and discharge current (A); and (d) duty cycle (C) and pulse on-time (B).

present the same influence on the TWR; increasing each of which makes the TWR increase progressively. This is undoubtedly due to the strong interactive nature of these two parameters suitably found by the ANOVA of TWR response (see Table 5). Moreover, the tool electrode suffers more from wear, where both the current and duty cycle are chosen at their high levels; a point located at the upper right part of Figure 7(b). Increasing duty cycle at a steady level of pulse on-time (the case where Figure 7(b) has been drawn) means lowering the pulse off-time, thus, increasing the frequency of electrical discharge assuring higher rates of electron attack on the anode tool electrode in a unit time [36,37].

Figure 7(c) displays the interactive effect of gap voltage and current on the TWR. As can be inferred, low TWRs (less than 0.02 g/h) may be accessible with the smallest level of current ($A = -1$) accompanied by every adjustable level of gap voltage. In other words, the coincident effects of these two factors on TWR counteract the effect of gap voltage alone (shown in Figure 5), as now the whole range of it can be selected to yield small TWRs provided that the current is kept low enough ($A = -1$). Figure 7(d) shows the concurrent effect of duty cycle and pulse on-time. It is obviously visible that small TWRs (below 0.03 g/h) can be obtained choosing the lowest level of duty cycle ($C = -1$) with a range of medium to high levels of pulse on-time ($0 < B < 1$). This combination confirms

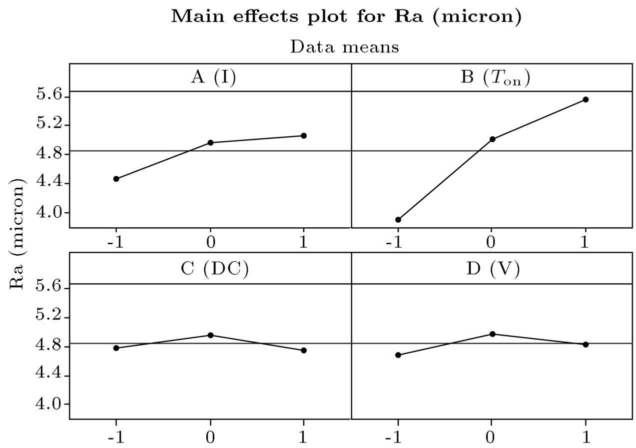

Figure 8. The main effects plot of input parameters over the Ra.

relatively decreased sparking frequency, meaning lower amounts of electron attack in a unit time to cause tool wear [36,37].

4.5. Main effect analysis of Ra

Figure 8 depicts the main effects plot of the four controllable parameters on the Ra. It is understandable that the first two variables, current and pulse on-time, have more influential impacts on the Ra than those of duty cycle and gap voltage. More specifically, increasing pulse on-time alone, while keeping the other factors constant at their middle levels, can increase the

Ra from 4 μm up to about 5.7 μm; a higher difference interval than that created by other parameters. As is also clear, altering both duty cycle and gap voltage, within their designated intervals considered in this research, causes little change of the Ra. This fact was also verified before (see Table 5), as not being significant parameters within 95% of confidence interval, and their main effects have just been shown here for comparative purposes. In general, the work surface quality in EDM depends primarily on the magnitude of electrical discharge energy governed mainly by current intensity and pulse on-time [31,32]. A prolonged pulse on-time makes the discharging action continue for a longer duration, so that broader craters are formed over the work surface, overwhelmed with an abundance of resolidified molten material not ejected effectively. This, in turn, leads to worsened and coarser surface quality [13].

4.6. Interaction effect analysis of Ra

Figure 9(a) illustrates the joint effects of pulse on-time and discharge current over the Ra. It is apparent that smoother surfaces can be obtained by assigning the lowest level of pulse on-time ($B = -1$), while providing a fair amount of discharge current. For example, if it is desired to produce a surface having a Ra roughness less than about 4 μm, then, it is feasible to choose any arbitrary value for the discharge current, within its investigated domain, provided that the pulse on-time is kept at its lowest level ($B = -1$). More noticeably, the combination of $B = -1$ and $A = 0$ gives the lowest Ra. Enough discharge current is needed to remove material from the high melting point WC-Co composite more effectively, with less remaining recast layer over the work piece, worsening the surface quality [31,32]. Figure 9(b) portrays the two-way interaction effects of gap voltage and discharge current. Under the circumstances in which this graph has been drawn, it can be concluded that the lowest value of Ra (about 4.2 μm) is achieved setting the highest level of gap voltage ($D = 1$), along with the minimum level of discharge current ($A = -1$). Higher gap voltage, while making the gap distance wider, facilitates debris removal from the gap space and can also help reduce electrical discharge density. Altogether, with low current intensity, they collaborate in attaining a superior surface quality [31,32].

5. Optimum selection of EDM parameters on WC/6%Co using desirability function technique

Metal removal rate is an indicator for productivity, while tool wear rate and surface finish account for process economics, precision, and work quality. In particular, tool wear is of paramount concern, especially when close tolerances in intricate geometries are needed. The EDM, as a complex and stochastic process, exhibits much difficulty in determining optimal machining parameters for best machining performance. The performance indicators, viz. MRR, TWR and Ra, are conflicting in nature, as it is always desirable to have higher MRR, with a lower value of surface roughness and tool wear rate, at the same time. Due to the presence of a large number of process variables and mutual interactions, the selection of optimum machining parameter combinations, to obtain higher MRR and smaller SR and TWR, is a challenging task [38]. Here, an attempt is made to develop a strategy based on the concept of desirability function for predicting the optimum machining parameter settings, generating maximum MRR, with minimum SR and TWR, all at once.

5.1. Optimization formulation

The mathematical formulation of the present optimization problem can be stated as follows:

$$\text{Max}: \ F_1(x) = \text{MRR};$$

$$\text{Min}: \ F_2(x) = \text{TWR};$$

$$\text{Min}: \ F_3(x) = \text{Ra}.$$

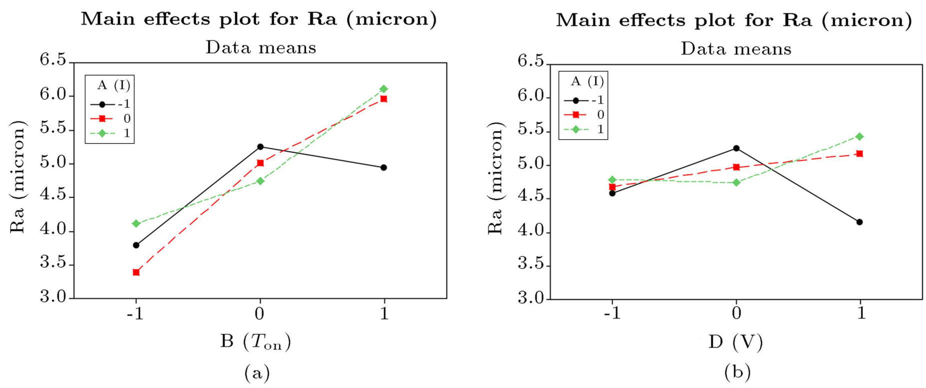

Figure 9. Interaction effect plots of Ra: (a) Pulse on-time (B) and discharge current (A); and (b) gap voltage (D) and discharge current (A).

Subject to :

$2 \leq x_1 \leq 8$

$50 \leq x_2 \leq 150$

$40 \leq x_3 \leq 80$

$$40 \leq x_4 \leq 80, \tag{21}$$

where x_1, x_2, x_3 and x_4 represent the input process parameters, I, T_{on}, DC and V, respectively. It is a four-variable-three-objective optimization statement, each of which has been defined by its respective second order regression equation (Eqs. (13)-(15)).

5.2. Optimization through desirability function

Popularized by Derringer and Suich [39], the Desirability Function Approach (DFA) is a kind of search-based optimization method capable of handling several response functions simultaneously to find optimal input settings, globally. The overall approach is to first convert each response, y_i into an individual desirability function, d_i, that varies over the range:

$$0 \leq d_i \leq 1. \tag{22}$$

If the response y_i is at its goal or target, then $d_i = 1$ (the most desirable case), and if the response is outside an acceptable region, then, $d_i = 0$ (the least desirable case). There is also a positive number, weight factor (r), associated with the desirability function of each response defining its shape. If the weight is chosen to be less than 1, then the sensitivity of the desirability function is low with respect to the optimal or target value sought for. In other words, if the search algorithm finds a point which is somehow far from the desired optimum or target value, then the decrease in desirability function value will be small in comparison to its maximum amount (unity). Choosing a weight factor higher than one has the reverse effect, and setting it to one provides a balanced or medium sensitivity with the shape of desirability being linear [24,25,40]. The individual desirability functions are defined according to the goal of optimization, i.e. maximization or minimization.

If the objective or target, T_i for the response, y_i, is a maximum value, then:

$$d_i = \begin{cases} 0 & y_i \prec L_i \\ \left(\frac{y_i - L_i}{T_i - L_i}\right)^r & L_i \leq y_i \leq T_i \\ 1 & y_i \succ T_i \end{cases} \tag{23}$$

and if the target for the response is a minimum value, then:

$$d_i = \begin{cases} 1 & y_i \prec T_i \\ \left(\frac{U_i - y_i}{U_i - T_i}\right)^r & T_i \leq y_i \leq U_i \\ 1 & y_i \succ U_i \end{cases} \tag{24}$$

where L_i and U_i represent the lower and upper limit values of the response, y_i, respectively.

The individual desirabilities are then combined to form the overall (composite or aggregated) desirability (D), another parameter varying between 0 and 1, as the weighted geometric mean of all the previously defined desirability functions, given by:

$$D = (d_1^{w_1} \times d_2^{w_2} \times d_3^{w_3} \times ... \times d_n^{w_n})^{\frac{1}{(w_1+w_2+w_3+...+w_n)}}$$

$$= (\Pi_{i=1}^{n} d_i^{w_i})^{\frac{1}{\Sigma_{i=1}^{n} w_i}}, \tag{25}$$

where w_i is of relative importance, a comparative scale for weighing each of the resulting d_i assigned to the ith response, and n is the number of responses ($n = 3$, in our case). The optimal settings are determined, so as to maximize overall desirability (D), usually by applying a reduced gradient algorithm with multiple starting points [40].

5.3. Parametric optimization of the EDM process on WC-6%Co

Based on the developed quadratic mathematical responses (Eqs. (13)-(15)), d_1, d_2, and d_3 are selected as the independent desirability functions for the MRR, TWR, and Ra, respectively. Moreover, the targets are placed on the MRR to become maximized, while TWR and Ra to be minimized. Unit weight factor ($r = 1$) and importance ($w_i = 1$) were also assigned for each response. The Response Optimizer option within the DOE module of the Minitab statistical software package, release 15, has been used here to search for the best set of optimum input parametric combinations, resulting in the most desirable compromise between different responses. Table 10 summarizes the key parameters set to find global optimum settings, including constraints of input variables and that of

Table 10. Constraints and criteria of input parameters and responses.

Parameter/Response	Goal	Lower limit	Upper limit
Discharge current	In range	2	8
Pulse on-time	In range	50	150
Duty cycle	In range	40	80
Gap voltage	In range	40	80
Material removal rate	Maximize	0.02	0.86
Tool wear rate	Minimize	0.007	0.15
Surface roughness	Minimize	3.395	6.589

Table 11. Iterative determination of optimum conditions (inputs in coded form).

Solution	Current (A)	Pulse on-time (B)	Duty cycle (C)	Gap voltage (D)	MRR (g/h)	TWR (g/h)	Ra (μm)	d_1	d_2	d_3	Composite desirability (D)
1	*0.232323*	*-0.989478*	*-1*	*-1*	*0.30187*	*0.04241*	*3.89837*	*1*	*1*	*1*	*1*
2	0.434343	-0.959596	-1	-0.959596	0.33782	0.05002	3.89841	1	0.999604	1	0.999868
3	-0.397059	-1	1	1	0.3	0.04763	3.94184	1	1	0.961959	0.987155
4	-0.501927	-0.942816	1	-1	0.32798	0.05	4.06218	1	1	0.852562	0.948219
5	0	-1	0	0.881845	0.3	0.05158	4.07341	1	0.96846	0.842356	0.934385
6	0.643528	-1	0.930431	0.419331	0.28849	0.05	4.16654	0.88494	0.999984	0.75769	0.875251
7	0.43614	-1	-0.599353	0.970432	0.27956	0.05	4.23107	0.79558 9	0.999998	0.699026	0.822357
8	-0.157129	-0.476585	1	1	0.32588	0.05	4.44991	1	1	0.500078	0.793742
9	0.997587	-1	-1	1	0.27054	0.0564	4.43547	0.705421	0.8719 67	0.513207	0.680895
10	0.344275	-0.15463	-0.946309	-1	0.28279	0.04136	4.64325	0.827884	1	0.324322	0.645132

Note: The first row in italic is selected as the best compromise solution.

response requirements, while Table 11 sorts the first ten optimum settings obtained in descending order of composite desirability (D). The closer D is to 1, the more favorable are the EDM conditions satisfying problem requirements. It can be seen from Table 11 that the most desirable operating conditions correspond to the first row and are discharge current $A = 0.2323$, pulse on-time $B = -0.9895$, duty cycle $C = -1$ and gap voltage $D = -1$ in coded form, equivalent to 5.70A, 50.53 μs, 40% and 40 V as real values, respectively. Accordingly, the optimized responses are 0.302 g/h, 0.042 g/h, and 3.898 μm for MRR, TWR, and Ra, respectively. A closer examination of the whole listed settings in Table 11 reveals that although higher MRRs can be obtained by other settings, those cases are subject to sacrificing both TWR and Ra, as they obtained higher values than those pertinent to the first solution. Figure 10 illustrates a visual representation

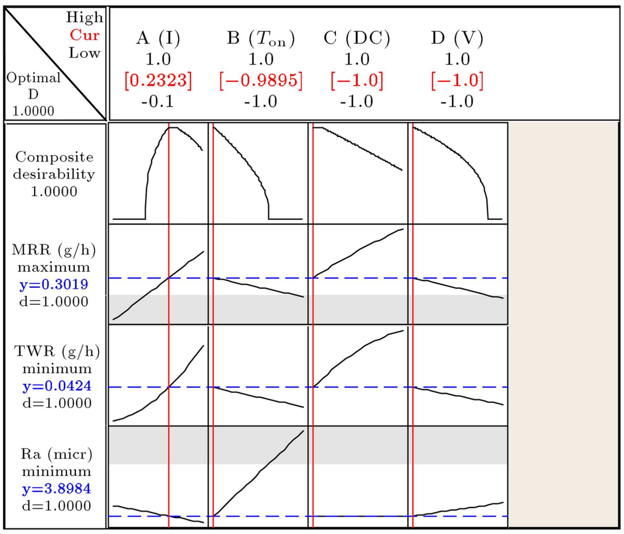

Figure 10. Final optimization results.

of the optimization result. The optimization plot shows the effect of each factor (columns) on the response or composite desirability (rows). Furthermore, each cell presents how the process output varies as a function of one of the process factors, while keeping the other parameters unchanged. Also, the vertical lines inside the cells show current optimal parametric settings, whereas the dotted horizontal lines represent the current response values. High and low settings of each process design variable can also be observed in this plot, denoted by 1 and -1, respectively. The most useful part is the optimal parameter settings required to achieve the process set target criteria, located in the middle row between the high and low rows, symbolized by "cur" and expressed in coded form. Finally, the first left column shows the composite, as well as all individual desirability, all being unity, along with optimum response values.

Conducting the confirmation experiment is the crucial, final, and indispensable part of every optimization attempt. A verification experiment was performed at the obtained optimal input parametric setting to compare the actual MRR, TWR, and Ra with those of optimal responses obtained through a desirability approach. Table 12 summarizes the optimization results, along with experimentally obtained responses, and their relative percentage verification errors.

As is clear, the amounts of error are all found to be satisfactory, from the point of engineering applications (10.64% as the worst case) in predicting the TWR, assuring the feasibility, predictability, and effectiveness of the adopted approach.

Moreover, these error values are also in good agreement with those represented in Table 9, all being in a comparable error margin for each response, proving that a consistent and reliable strategy has been employed in this research.

Table 12. Multi-response optimal points and experimental validation.

Optimum input setting				MRR (g/hr)		TWR (g/hr)		Ra (μm)		Relative prediction error (%)		
I (A)	T_{on} (μs)	DC (%)	V (V)	Predicted	Exp.[a]	Predicted	Exp.[a]	Predicted	Exp.[a]	MRR	TWR	Ra
5.70	50.53	40	40	0.302	0.331	0.042	0.047	3.898	4.141	8.76	10.64	5.87

[a]: Experimental.

5.4. The interpretation of optimal settings

Making a thorough analysis of the optimum input values can provide a fair basis to justify their estimated amounts from the point of physical aspects involved in the EDM process. In the course of optimization through the desirability function approach, a measure of how well the solution has satisfied the combined goals for all responses must be assured. That is, $D = 1$, and the optimum setting providing this could have been able to make a tradeoff between different objective functions. The amount of optimal discharge current has been found to be near its middle value, providing fair electro-thermal energy, so that neither a very low MRR nor an extremely high one is obtained. Along with almost the shortest possible pulse on-time (50.53 μs), the existence of adequate electrical discharge density is assured to help maintain enough impulsive force to expel much of the molten material from the crater [38,11]. Moreover, as was discussed in subsection 4.5, shorter pulse on-times are in favor of smoother surfaces, as the resulted craters' dimensions (depth and diameter) are smaller compared with those created with long pulse durations. Hence, better surface quality is guaranteed. Finally, the optimal values of duty cycle and gap voltage are equivalent to their lowest possible levels considered in the experimental plan, as increasing either of them may cause the process performance to deviate from its optimum condition by sacrificing any of the three responses. This effect can be seen in Table 11. Especially, the lowest gap voltage (40 V) provides a narrower gap distance, increasing the electrical discharge density inside the gap zone, which, in turn, helps improve the MRR.

6. Conclusions

Conventional machining of the hard metal WC/6%Co composite is extremely laborious, burdensome, and time consuming, due to its elevated hardness and brittleness over a wide range of temperatures and working conditions. The effective and economic utilization of the EDM process on such a material, with optimum selection of input parameters, needs a thorough understanding of its machinability behavior, which, in turn, can substantially alleviate the difficulties encountered. In short, based on in-depth and comprehensive analysis and optimization of WC-6%Co ED-machinability indices, the following principal conclusions can be drawn:

1. All the main effects of input parameters, i.e. discharge current, pulse on-time, duty cycle and gap voltage, have been found to be highly significant, affecting both the MRR and TWR. However, for the third response, Ra, just the main effects of the first two were revealed to be statistically important.
2. Regarding the main effects analysis, both the MRR and TWR behave in the same way. However, the TWR behaves more nonlinearly. Increasing either discharge current or duty cycle results in higher values of stock removal rate and tool wear, whereas increasing pulse on-time or gap voltage causes the reverse effect. On the other hand, the work roughness value, Ra, is directly proportional to both the discharge current and pulse on-time, while the main effects of the other parameters were found to be negligible.
3. The two way interaction effects of discharge current with pulse on-time ($A \times B$), duty cycle ($A \times C$), and gap voltage ($A \times D$), as well as the interaction between the pulse on-time with duty cycle ($B \times C$) and pure quadratic effect of duty cycle (C^2), have all been found to significantly influence the MRR.
4. On measuring TWR, the same dual interaction effects influencing the MRR, plus the pure quadratic effect of discharge current (A^2), were understood to be statistically significant.
5. For the Ra response, the interactions between discharge current with pulse on-time ($A \times B$) and discharge current with gap voltage ($A \times D$) possess significant effects.
6. Higher MRRs are always accessible through either enhancing electrical discharge density or rising sparking frequency. These conditions are feasible by lowering the pulse on-time and gap voltage or increasing duty cycle, while considering larger discharge currents to confirm greater released electro-thermal energy as a result of sparking.
7. Low amounts of TWR can mainly be obtained by a combination of lower current levels with prolonged pulse on-times or longer pulse on-times

with smaller duty cycles. Decreased discharging frequency resulted from longer pulse durations can help protect the anode tool from serious wear, as a smaller number of discharges take place within a unit of time. In other words, positive ions get enough time with a longer pulse on-time to reach the cathode workpiece, while occupying much of the path within the discharge channel, and not allowing high volumes of electrons to easily bombard the anode tool.

8. Smoother surfaces can be produced via a combination of either low current intensity with shorter pulse on-time or low current level with higher gap voltage. While keeping the discharge current low enough, the first case produces shallower craters with smaller diameters, while the latter gives rise to wider gap size. This helps facilitate better debris evacuation and less deposition of molten products on the work surface, hence, improving the surface quality in either case.
9. The superior optimum operating conditions that can simultaneously bring out maximum MRR and minimum TWR and Ra are 5.70 A, 50.53 μs, 40%, and 40 V as current, pulse on-time, duty cycle and gap voltage, respectively. By verifying these optimized points, the worst relative error is revealed as 10.640% between the predicted optimal and experimentally obtained values of TWR.
10. Though the EDM process parameters on WC-6%Co are highly interconnected, due to its inherently complex and stochastic nature, the approach of RSM coupled with DF can beneficially help identify process behavior and determine appropriate EDM conditions meeting all performance criteria in a compromised manner.

Nomenclature

A	Discharge current I (amperes)
Adj MS	Adjusted Mean Square
Adj SS	Adjusted Sum of Squares
B	Pulse on-time T_{on} (microsecond)
C	Average gap voltage V (volts)
D	Duty cycle (%), composite desirability
d_i	Desirability for ith response
DC	Duty Cycle
DF	Degree of Freedom
e_i	ith residual
I_{dis}	Discharge current
J	Electrical discharge density of plasma channel
k	Number of independent process variables
L_i	Lower value of the ith response
MRR	Material Removal Rate (grams per hour: g/h)
MS_{Res}	Residual mean square
MS_T	Total mean square
N	Total number of experiments, total number of discharge pulses
n_a	Number of axial (star) points
n_c	Number of center points
n_f	Number of factorial points
PRESS	Prediction error sum of squares
q	Discharge energy per pulse
Q	Total discharge energy
Ra	Average surface roughness (micrometer)
R^2	Coefficient of determination (R-squared)
R^2_{Adj}	Adjusted R-squared
R^2_{Pred}	Predicted R-squared
Seq SS	Sequential sum of squares
SS_{Res}	Residual sum of squares
SS_T	Total sum of squares
T	Total machining time
T_d	Ignition delay time
T_D	Total discharge duration
T_i	Target for the ith response
T_{off}	Pulse off-time
TWR	Tool Wear Rate (grams per hour: g/h)
V_{dis}	Discharge voltage
U_i	Upper value of the ith response
y_i	ith response parameter

References

1. Abbas, N.M., Solomon, D.G. and Fuad Bahari, M.d. "A review on current research trend in electrical discharge machining (EDM)", *Int. J. Mach. Tools and Manufact.*, **47**, pp. 1214-1228 (2007).
2. Ho, K.H. and Newman, S.T. "State of the art electrical discharge machining (EDM)", *Int. J. Mach. Tools and Manufact.*, **43**, pp. 1287-1300 (2003).
3. Peças, P. and Henriques, E. "Intrinsic innovations of die sinking electrical discharge machining technology: estimation of its impact", *Int. J. Adv. Manuf. Technol.*, **44**, pp. 880-889 (2009).
4. Kuppan, P., Rajadurai, A. and Narayanan, S. "Influence of EDM process parameters in deep hole drilling of Inconel 718", *Int. J. Adv. Manuf. Technol.*, **38**(1-2), pp. 74-84 (2008).

5. Gu, L., Li, L., Zhao, W. and Rajurkar, K.P. "Electrical discharge machining of Ti6Al4V with a bundled electrode", *Int. J. Mach. Tools and Manufact.*, **53**(1), pp. 100-106 (2012).

6. Yildiz, Y., Sundaram, M.M. and Rajurkar, K.P. "Optimization study and statistical analysis on the machinability of beryllium-copper (Be-Cu) alloy in EDM", *Proc. IMechE Part B: Journal of Engineering Manufacture*, **226**(11), pp. 1847-1861 (2012).

7. Garg, R.K., Singh, K.K., Sachdeva, A., Sharma, V.S., Ojha, K. and Singh, S. "Review of research work in sinking EDM and WEDM on metal matrix composite materials", *Int. J. Adv. Manuf. Technol.*, **50**(5-8), pp. 611-624 (2010).

8. Gopalakannan, S. and Senthilvelan, T. "EDM of cast Al/SiC metal matrix nanocomposite by applying response surface method", *Int. J. Adv. Manuf. Technol.*, **67**, pp. 485-493 (2013).

9. Luis, C.J. and Puertas, I. "Methodology for developing technological tables used in EDM processes of conductive ceramics", *J. Mater. Process Technol.*, **189**(1-3), pp. 301-309 (2007).

10. Rajurkar, K.P., Levy, G., Malshe, A., Sundaram, M.M., McGeough, J., Hu, X., Resnick, R. and DeSilva, A. "Micro and nano machining by electro-physical and chemical processes", *Ann. CIRP*, **55**(2), pp. 643-666 (2006).

11. Kunieda, M., Lauwers, B., Rajurkar, K.P. and Schumacher, B.M. "Advancing EDM through fundamental insight into the process", *Ann. CIRP*, **54**(2), pp. 599-622 (2005).

12. Jahan, M.P., Rahman, M. and Wong, Y.S. "A review on the conventional and micro-electro discharge machining of tungsten carbide", *Int. J. Mach. Tools and Manufact.*, **51**, pp. 837-858 (2011).

13. Mahdavinejad, R.A. and Mahdavinejad, A. "ED machining of WC-Co", *J. Mater. Process Technol.*, **162-163**, pp. 637-643 (2005).

14. Abdullah, A., Shabgard, M.R., Ivanov, A. and Shervanyi-Tabar, M.T. "Effect of ultrasonic-assisted EDM on the surface integrity of cemented tungsten carbide (WC-Co)", *Int. J. Adv. Manuf. Technol.*, **41**, pp. 268-280 (2009).

15. Lee, S.H. and Li, X.P. "Study of the effect of machining parameters on the machining characteristics in electrical discharge machining of tungsten carbide", *J. Mater. Process Technol.*, **115**, pp. 344-358 (2001).

16. Lee, S.H. and Li, X. "Study of the surface integrity of the machined workpiece in the EDM of tungsten carbide", *J. Mater. Process Technol.*, **139**, pp. 315-321 (2003).

17. Puertas, I., Luis, C.J. and Álvarez, L. "Analysis of the influence of EDM parameters on surface quality, MRR and EW of WC-Co", *J. Mater. Process Technol.*, **153-154**, pp. 1026-1032 (2004).

18. Puertas, I. and Luis, C.J. "A study on the electrical discharge machining of conductive ceramics", *J. Mater. Process Technol.*, **153-154**, pp. 1033-1038 (2004).

19. Lin, Y.C., Chen, Y.F., Lin, C.T. and Tzeng, H.Y. "Electrical discharge machining (EDM) characteristics associated with electrical discharge energy on machining of cemented tungsten carbide", *Materials and Manufacturing Processes*, **23**, pp. 391-399 (2008).

20. Kanagarajan, D., Karthikeyan, R., Palanikumar, K. and Sivaraj, P. "Influence of process parameters on electric discharge machining of WC/30%Co composite", *Proc. IMechE, Part B: J. Engineering Manufacture*, **222**, pp. 807-815 (2009).

21. Kanagarajan, D., Karthikeyan, R., Palanikumar, K. and Davim, J.P. "Optimization of electrical discharge machining characteristics of WC/Co composite using non-dominated sorting genetic algorithm (NSGA-II)", *Int. J. Adv. Manuf. Technol.*, **36**, pp. 1124-1132 (2008).

22. Banerjee, S., Mahapatro, D. and Dubey, S. "Some study on electrical discharge machining of ({WC+TiC+TaC/NbC}-Co) cemented carbide", *Int. J. Adv. Manuf. Technol.*, **43**, pp. 1177-1188 (2009).

23. Puertas, I. and Luis, C.J. "Optimization of EDM conditions in the manufacturing process of B4C and WC-Co conductive ceramics", *Int. J. Adv. Manuf. Technol.*, **59**(5-8), pp. 575-582 (2012).

24. Montgomery, D.C., *Design and Analysis of Experiments*, 7th Edition, Wiley, New York, USA (2009).

25. Myers, R.H. and Montgomery, D.C., *Response Surface Methodology*, 2nd Edition, Wiley, New York, USA (2002).

26. Montgomery, D.C., Peck, E.A. and Vining, G.G., *Introduction to Linear Regression Analysis*, 5th Edition, Wiley Interscience, Hoboken, New Jersey, USA (2012).

27. Assarzadeh, S. and Ghoreishi, M. "Statistical modeling and optimization of process parameters in electro-discharge machining of cobalt-bonded tungsten carbide composite (WC/6%Co)", *Procedia CIRP*, **6**, pp. 464-469 (2013).

28. Jain, V.K. *Advanced Machining Processes*, Allied Publishers, New Delhi, India (2004).

29. McGeough, J.A. *Advanced Methods of Machining*, Chapman and Hall, New York, USA (1988).

30. Habib, S.S. "Study of the parameters in electrical discharge machining through response surface methodology approach", *Appl. Math. Modelling*, **33**(12), pp. 4397-4407 (2009).

31. Assarzadeh, S. and Ghoreishi, M. "Neural-network-based modeling and optimization of the electro-discharge machining process", *Int. J. Adv. Manuf. Technol.*, **39**(5-6), pp. 488-500 (2008).

32. Assarzadeh, S. and Ghoreishi, M. "A dual response surface-desirability approach to process modeling and optimization of Al_2O_3 powder-mixed electrical discharge machining (PMEDM) parameters", *Int. J. Adv. Manuf. Technol.*, **64**(9-12), pp. 1459-1477 (2013).

33. Zhang, J.H., Lee, T.C., Wu, C.L. and Tang, C.Y. "Surface integrity and modification of electro-discharge machined alumina-based ceramic composite", *J. Mater. Process Technol.*, **123**, pp. 75-79 (2002).

34. DiBitonto, D.D., Eubank, Ph.T., Patel, M.R. and Barrufet, M.A. "Theoretical models of the electrical discharge machining process. I. A simple cathode erosion model", *J. Appl. Phys.*, **66**(9), pp. 4095-4103 (1989).

35. Amorim, F.L. and Weingaerner, W.L. "Influence of duty factor on the die-sinking electrical discharge machining of high-strength aluminum alloy under rough machining", *J. of the Braz. Soc. Mechanical Sciences,* **XXIV**, pp. 194-199 (2002).

36. Jameson, E.C., *Electrical Discharge Machining: Tooling, Methods and Applications*, Society of Manufacturing Engineers (SME), USA (2001).

37. Yoo, B.H., Min, B.K. and Lee, S.J. "Analysis of the machining characteristics of EDM as functions of the mobilities of electrons and ions", *Int. J. of Precision Engineering and Manufacturing*, **11**(4), pp. 629-632 (2010).

38. Schumacher, B.M. "After 60 years of EDM the discharge process remains still disputed", *J. Mater. Process Technol.*, **149**, pp. 376-381 (2004).

39. Derringer, G. and Suich, R. "Simultaneous optimization of several response variables", *J. Qual. Technol.*, **12**(4), pp. 214-219 (1980).

40. Castillo, E.D., Montgomery, D.C. and McCarville, D.R. "Modified desirability functions for multiple response optimization", *J. Qual. Technol.*, **28**(3), pp. 337-345 (1996).

Biographies

Saeed Assarzadeh obtained BS and MS degrees in Mechanical Engineering from Ferdowsi University of Mashhad, Iran, and K. N. Toosi University of Technology, Tehran, Iran, respectively, and is currently a final year PhD student in the Department of Mechanical Engineering at K. N. Toosi University of Technology, Tehran, Iran.

Majid Ghoreishi obtained BS and MS degrees in Mechanical Engineering from Sharif University of Technology, Tehran, Iran, and a PhD degree, in the area of nontraditional machining, from Manchester University, Institute of Science and Technology (UMIST), UK, in 2001. He is currently Associate Professor in the Faculty of Mechanical Engineering at K. N. Toosi University of Technology, Tehran, Iran.